university of groningen

University Medical Center Groningen

University of Groningen

Triphenylene-Derived Electron Acceptors and Donors on Ag(111)

Müller, Kathrin; Schmidt, Nico; Link, Stefan; Riedel, Rene; Bock, Julian; Malone, Walter ; Lasri, Karima; Kara, Abdelkader; Starke, Ulrich; Kivala, Milan

Published in:
Small

DOI:
10.1002/smll.201901741

IMPORTANT NOTE: You are advised to consult the publisher's version (publisher's PDF) if you wish to cite from it. Please check the document version below.

Document Version
Publisher's PDF, also known as Version of record

Publication date:
2019

Link to publication in University of Groningen/UMCG research database

Citation for published version (APA):
Müller, K., Schmidt, N., Link, S., Riedel, R., Bock, J., Malone, W., Lasri, K., Kara, A., Starke, U., Kivala, M., & Stöhr, M. (2019). Triphenylene-Derived Electron Acceptors and Donors on Ag(111): Formation of Intermolecular Charge-Transfer Complexes with Common Unoccupied Molecular States. *Small*, *15*(33), [1901741]. https://doi.org/10.1002/smll.201901741

Copyright
Other than for strictly personal use, it is not permitted to download or to forward/distribute the text or part of it without the consent of the author(s) and/or copyright holder(s), unless the work is under an open content license (like Creative Commons).

The publication may also be distributed here under the terms of Article 25fa of the Dutch Copyright Act, indicated by the “Taverne” license. More information can be found on the University of Groningen website: https://www.rug.nl/library/open-access/self-archiving-pure/taverne-amendment.

Take-down policy
If you believe that this document breaches copyright please contact us providing details, and we will remove access to the work immediately and investigate your claim.

Downloaded from the University of Groningen/UMCG research database (Pure): http://www.rug.nl/research/portal. For technical reasons the number of authors shown on this cover page is limited to 10 maximum.

Download date: 05-05-2023

NANO · MICRO small
www.small-journal.com

Triphenylene-Derived Electron Acceptors and Donors on Ag(111): Formation of Intermolecular Charge-Transfer Complexes with Common Unoccupied Molecular States

Kathrin Müller, Nico Schmidt, Stefan Link, René Riedel, Julian Bock, Walter Malone, Karima Lasri, Abdelkader Kara, Ulrich Starke, Milan Kivala,* and Meike Stöhr**

Over the past years, ultrathin films consisting of electron donating and accepting molecules have attracted increasing attention due to their potential usage in optoelectronic devices. Key parameters for understanding and tuning their performance are intermolecular and molecule–substrate interactions. Here, the formation of a monolayer thick blend of triphenylene-based organic donor and acceptor molecules from 2,3,6,7,10,11-hexamethoxytriphenylene (HAT) and 1,4,5,8,9,12-hexaazatriphenylenehexacarbonitrile (HATCN), respectively, on a silver (111) surface is reported. Scanning tunneling microscopy and spectroscopy, valence and core level photoelectron spectroscopy, as well as low-energy electron diffraction measurements are used, complemented by density functional theory calculations, to investigate both the electronic and structural properties of the homomolecular as well as the intermixed layers. The donor molecules are weakly interacting with the Ag(111) surface, while the acceptor molecules show a strong interaction with the substrate leading to charge transfer and substantial buckling of the top silver layer and of the adsorbates. Upon mixing acceptor and donor molecules, strong hybridization occurs between the two different molecules leading to the emergence of a common unoccupied molecular orbital located at both the donor and acceptor molecules. The donor acceptor blend studied here is, therefore, a compelling candidate for organic electronics based on self-assembled charge-transfer complexes.

1. Introduction

Organic molecules are considered highly valuable for applications ranging from organic light emitting diodes[1] over organic photovoltaics[2] to field effect transistors[3] and molecular sensors.[4] Such compounds are used as active materials in a variety of devices due to their low costs, easy processability, light weight, structural flexibility, and tunability of their electronic properties by chemical synthesis.[5] However, the rather weak van der Waals interactions, which often govern the intermolecular interactions, substantially limit the performance of today's devices.

In order to unravel the interplay of intermolecular and molecule–substrate interactions, which play a key role in the device performance, considerable fundamental research on homomolecular layers on different metal substrates has been performed over the last three decades.[6,7] In contrast, studies on the electronic and structural properties of binary systems have only emerged in the last few years.[8–10] Special focus has been put on the organic–inorganic and organic–organic interface, which determines key properties like contact resistance, charge injection, and extraction.[7,11]

One approach for increasing the intermolecular interactions is based on the decoration of the organic molecules with complementary functional groups, e.g., hydrogen-bond donating and accepting groups.[10,12] In the last few years, the use of fluorinated molecules in mixed molecular layers leading to hydrogen-fluorine bonds was studied intensely.[13–16] Besides the increased intermolecular interaction

Dr. K. Müller, Dr. N. Schmidt, Prof. M. Stöhr
Zernike Institute for Advanced Materials
University of Groningen
Nijenborgh 4, 9747 AG Groningen, Netherlands
E-mail: k.mueller@fkf.mpg.de; m.a.stohr@rug.nl

The ORCID identification number(s) for the author(s) of this article can be found under https://doi.org/10.1002/smll.201901741.

© 2019 The Authors. Published by WILEY-VCH Verlag GmbH & Co. KGaA, Weinheim. This is an open access article under the terms of the Creative Commons Attribution-NonCommercial License, which permits use, distribution and reproduction in any medium, provided the original work is properly cited and is not used for commercial purposes.

DOI: 10.1002/smll.201901741

Dr. K. Müller, Dr. S. Link, Prof. U. Starke
Max Planck Institute for Solid State Research
Heisenbergstrasse 1, D-70569 Stuttgart, Germany

R. Riedel
Department of Chemistry and Pharmacy
University of Erlangen-Nürnberg
Nikolaus-Fiebiger-Strasse 10, D-91058 Erlangen, Germany

J. Bock, Prof. M. Kivala
Organisch-Chemisches Institut & Centre for Advanced Materials
Ruprecht-Karls-Universität Heidelberg
Im Neuenheimer Feld 270 & 225, 69120 Heidelberg, Germany
E-mail: milan.kivala@oci.uni-heidelberg.de

W. Malone, Dr. K. Lasri, Prof. A. Kara
Department of Physics
University of Central Florida
Orlando, FL 32816, USA

© 2019 The Authors. Published by WILEY-VCH Verlag GmbH & Co. KGaA, Weinheim

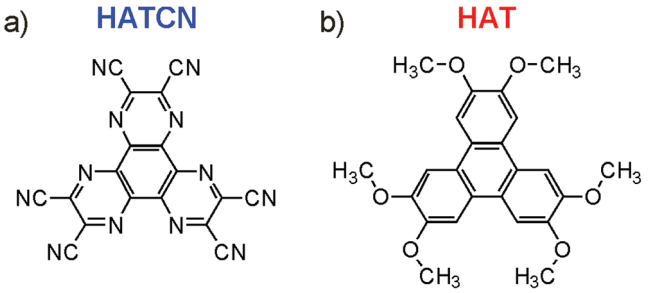

Scheme 1. Molecular structures of: a) HATCN (1,4,5,8,9,12-hexaazatriphenylenehexacarbonitrile) and b) HAT (2,3,6,7,10,11-hexamethoxytriphenylene).

of fluorinated molecules with hydrogen-bond donating molecules, the fluorination induces electron accepting character and based on their hydrogen-fluorine bonds, strong intermolecular interaction can be achieved.[17–20] Consequently, the resulting intermixed layers often exhibited similar self-assembly patterns independent of the underlying metal substrate.[9] However, the electronic structure is only slightly affected by the intermixing, resulting in a rigid shift of the electronic states in the intermixed layers compared to the homomolecular ones but a strong hybridization leading, e.g., to common electronic states was not observed for these systems.[9,14,20–22]

One of the first examples where monolayer thick films of electronically strongly interacting mixtures of donor and acceptor molecules were investigated is the case of tetrathiafulvalene/tetracyanoquinodimethane (TTF/TCNQ).[23] These molecules form a 3D bulk charge-transfer salt exhibiting metallic properties with a conductivity of $1.47 \times 10^4\ \Omega^{-1}\ cm^{-1}$.[24] On an Au(111) surface it was reported that a dispersing quasi 1D band along the TCNQ molecules exists. Its origin lies in a complex mixing of metal and molecular states giving rise to a new interface state, which cannot be explained by the electronic properties of the pristine molecular components.[23]

Recently, a number of other charge-transfer (CT) complexes—thin films as well as crystalline samples—were investigated by means of ultraviolet photoelectron spectroscopy (UPS), X-ray photoelectron spectroscopy (XPS), near-edge X-ray absorption fine structure (NEXAFS) measurements, and density functional theory (DFT) calculations.[25–27] In these studies, mostly evaporated or solution-processed samples exploring TCNQ as an acceptor and pyrene derivatives as a donor,[25,26] or coronene derivatives for both acceptor and donor,[27] were investigated. For the coronene derivatives, the core level binding energy of the donor shifted toward higher binding energy and that of the acceptor shifted toward lower binding energy upon mixing, indicating a weak CT system.[27] In contrast, for microcrystals grown from pyrene and TCNQ additional peaks were observed in the XPS and NEXAFS spectra indicating a hybridization of specific orbitals and ionization of the molecules due to charge transfer.[25]

In this paper, we report on an organic binary donor–acceptor system consisting of two molecules, which exhibit threefold rotational symmetry and complementary electronic properties. As electron acceptor we used 1,4,5,8,9,12-hexaazatriphenylenehexacarbonitrile (HATCN; **Scheme 1**a),[28] while electron-rich 2,3,6,7,10,11-hexamethoxytriphenylene (HAT; Scheme 1b), known for its good electron donating

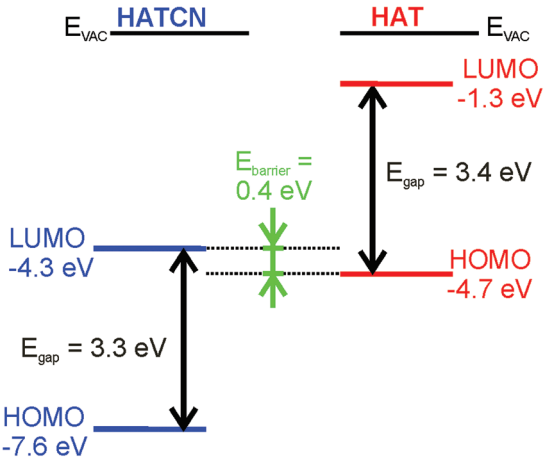

Figure 1. Schematic view of the energy levels of HATCN (left) and HAT (right). The bandgaps are taken from the UV–vis data, the LUMO of HATCN was derived from the CV curves and the HOMO and LUMO of HAT are taken from ref. [30].

properties when in contact with a strong acceptor, was used as the second component.[29] The complementary character of the two molecules facilitated a well-ordered assembly in the mixed layer as observed by scanning tunneling microscopy (STM) and low-energy electron diffraction (LEED). Using scanning tunneling spectroscopy (STS), we identified a common unoccupied state distributed across both molecules, which was absent for either of the homomolecular layers. These results point to a strong hybridization within the intermixed molecular layers. Our HATCN-HAT system, thus, represents a new strong candidate for organic (opto)electronic applications based on CT complexes.

2. Results

2.1. Structural and Electronic Properties of HAT and HATCN

Before discussing the adsorption on Ag(111), the structural and electronic properties of HAT and HATCN are briefly described. Our DFT calculations show that the molecular backbone of the HATCN is planar in the gas phase. The HAT molecule can exist in different conformations due to the rotational flexibility of the O-CH_3 groups. Scheme 1b illustrates one of the most stable conformations, which also exhibits a flat molecular backbone. In contrast, the conformation where two O-CH_3 groups are rotated shows a slight buckling and consequently is 225 meV less stable (Figure S1a,b, Supporting Information). The calculation of the density of states (DOS) of these two different conformations shows no difference in the highest occupied molecular orbital (HOMO) and lowest unoccupied molecular orbital (LUMO) and only slight modifications at the lower lying states (Figure S1c, Supporting Information).

Figure 1 shows the energy diagrams of the two molecules derived from our electrochemical and UV–vis measurements (see Figure S2 and Table S1, Supporting Information). The HOMO of the HAT molecule is found at 4.7 eV below the vacuum level while the LUMO of HATCN resides at 4.3 eV

© 2019 The Authors. Published by WILEY-VCH Verlag GmbH & Co. KGaA, Weinheim

below the vacuum level. This leads to a charge injection barrier of only 0.4 eV for a charge transfer from the HOMO of HAT into the LUMO of HATCN. These values compare rather well with energy values derived from optical and electrochemical measurements.[30,31] The positions of the energy levels highlight the electronic complementarity of HATCN and HAT and their excellent suitability to form CT complexes.

2.2. Self-Assembly of the Molecules

In the following, we describe the self-assembly of the homomolecular layers as well as the blend of HATCN and HAT on the Ag(111) surface. For coverages ≤1 monolayer (ML), HATCN molecules formed a porous hexagonal network. In the close-up STM image presented in **Figure 2**a, the triangular shape arising from the hexaazatriphenylene-backbone of the molecules is clearly visible. As known from literature, STM generally does not image the cyano groups.[32] Dislocation lines and stacking faults interrupted the long-range order (see Figure S3a, Supporting Information). No mirror or rotational domains were observed in the STM images. The LEED pattern (Figure 2a, top right) displays a (7×7) superstructure which is in line with the absence of rotational domains. Combining the information from LEED and STM and using the lattice constant of Ag (4.09 Å), the unit cell can be described by $a = b = 2.02$ nm and an enclosing angle of $\theta = 120°$. The tentative structure model (Figure 2a, bottom right), which was derived from the STM and LEED observations, demonstrates that the molecular network is stabilized by dipolar coupling between the negatively charged N-atoms and the positively charged C-atoms of neighboring cyano groups.[33] Our DFT calculations of the (7×7) superstructure on Ag(111) illustrate a similar self-assembled arrangement with a molecule–molecule distance of 1.2 nm (Figure S4a, Supporting Information). The adsorption energy is 2.41 eV per molecule and the average adsorption height of the carbon atoms is 3.18 Å and of the nitrogen atoms is 3.03 Å (Table S2, Supporting Information). Furthermore, the DFT calculations indicate that the cyano groups are significantly bent toward the substrate leading to a strong buckling of the molecule as well as of the top surface layer visible in the difference between the lowest and highest Z positions of Ag and N, respectively. Our findings for HATCN on Ag(111) are in line with those reported by Glowatzki et al.[34]

For coverages ≤1 ML, HAT molecules assembled into a hexagonal close-packed network as depicted in Figure 2b. In the STM images, individual molecules appear with six protrusions at their periphery. These "legs" derive from the six methoxy groups of the molecule. From the mirror-symmetric shape of the molecules, it can be inferred that the molecules are adsorbed in conformation 1 shown in Scheme 1b. For room temperature measurements, HAT was found to be mobile and the aforementioned network could only be observed for monolayer coverages. However, when measuring at 77 K, HAT molecules formed hexagonally close packed islands of several hundred nanometers in size with only a few vacancies (Figure S3b, Supporting Information). Occasionally, also 1D molecular wires were observed. This was especially the case for low coverages as demonstrated in Figure S5 in the Supporting Information. From the LEED

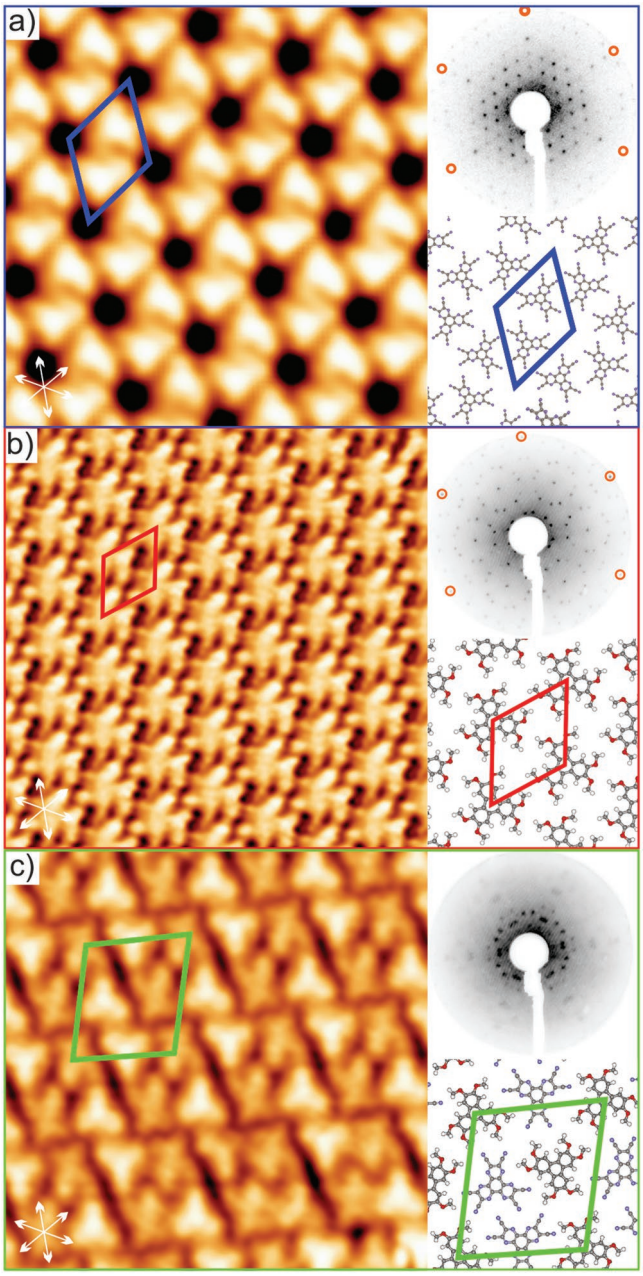

Figure 2. Self-assembly of a) HATCN, b) HAT, and c) HAT+HATCN on Ag(111). The substrate orientation is indicated by white arrows in the STM images. STM parameters: a) $T = 77$ K, $U = 0.5$ V, $I = 150$ pA, 8×8 nm^2; b) $T = 77$ K, $U = 0.2$ V, $I = 30$ pA, 8×8 nm^2; c) $T = 77$ K, $U = 0.5$ V, $I = 40$ pA, 8×8 nm^2. Positive bias refers to tunneling into unoccupied states of the samples. Top right: LEED patterns taken at 36 eV (a), 37 eV (b) and 15 eV (c); in a) and b) the substrate spots are indicated by orange circles (in c) they are located outside the screen). Bottom right: tentative structure models; the unit cells are indicated in blue, red, and green for a), b) and c), respectively.

pattern (Figure 2b, top right) a $\left(\sqrt{21} \times \sqrt{21}\right) R10.9°$ superstructure for HAT on Ag(111) was determined, which can be also described by a $\begin{pmatrix} 5 & 1 \\ -1 & 4 \end{pmatrix}$ matrix. Thus, two mirror domains rotated by ±10.9° with respect to the Ag [1–10] direction were

© 2019 The Authors. Published by WILEY-VCH Verlag GmbH & Co. KGaA, Weinheim

present on the surface (see white arrows in Figure 2b for the substrate unit cell direction). The unit cell vectors of this network derived from the LEED data are $a = b = 1.32$ nm with an enclosing angle of $\theta = 120°$. The tentative structure model in Figure 2b, bottom right shows one of the mirror domains. It is apparent that the molecular assembly is stabilized by hydrogen bonding between the hydrogen atoms of the methyl groups and neighboring oxygen atoms. This self-assembly pattern agrees with our DFT calculations, which showed a similar molecular orientation (Figure S4b, Supporting Information). Moreover, our DFT calculations give an adsorption energy for HAT of 2.27 eV per molecule and show that the molecular backbone of HAT adsorbs rather flat on the surface with an average adsorption height of the carbon atoms of 3.34 Å and for the oxygen atoms of 3.38 Å (Table S3, Supporting Information). The lower adsorption energy and higher adsorption height of HAT compared to HATCN indicates that the latter interacts somewhat more strongly with the Ag(111) surface than the former.

To facilitate successful intermixing of both molecules on the silver surface, HAT molecules were deposited first. Due to their high mobility at room temperature for sub-monolayer coverage, they could easily mix with the added HATCN molecules. After depositing an approximate one-to-one ratio of HAT and HATCN on Ag(111), a close-packed network formed as illustrated in Figure 2c. In large-scale STM images, a row-like pattern emerges (Figure S3c, Supporting Information). The close-up view in Figure 2c clearly indicates two differently appearing molecules. The brighter molecules exhibit a triangular shape while the dark molecules possess an asymmetric cross-like shape. The bright, triangular molecules could be identified as the HATCN molecules as they exhibit the same appearance as in the pure HATCN layer (Figure 2a). In contrast, the darker, asymmetric molecules do not display the six symmetrically arranged "legs" observed for the pure HAT layer. The reason for this different appearance lies in the rotational flexibility of the methoxy groups of HAT, leading to several possible conformations. In the conformation present in the binary layer, two of the methyl groups are rotated toward the neighboring methoxy groups while for one of the phenyl rings both methyl legs are oriented to the outside. This specific conformation, which is shown in Figure S1b in the Supporting Information, leads to an asymmetric cross-like appearance seen in the STM image. The LEED pattern (Figure 2c, top right) is more complex than for the homomolecular assemblies. We propose that the intermixed molecular layer formed an incommensurate superstructure, since there is no integer matrix, which can describe the observed LEED pattern. The lengths of the unit cell vectors were only determined from STM data and measured $a = 2.4 \pm 0.1$ nm and $b = 2.7 \pm 0.1$ nm with an enclosing angle of $\theta = 103 \pm 3°$.[35] The observed adsorption pattern gives rise to six rotational domains on the surface. In the tentative structure model (Figure 2c, bottom right) most cyano groups of a HATCN molecule form H-bonds with neighboring HAT molecules, while one cyano group undergoes dipolar coupling with another HATCN molecule. The dipolar coupling interaction is similar to the one observed for homomolecular HATCN structures. The unit cell contains two HATCN and two HAT molecules as indicated by the green tetragon in the tentative structure model (Figure 2c, bottom right).

Unfortunately, it was not possible to perform DFT calculations on the intermixed unit cell on Ag(111) due to its incommensurability and huge size. However, we placed one HATCN and one HAT molecule close to each other on the Ag(111) surface (see Figure S4c, Supporting Information) in order to gain additional insight into the structural properties when mixing both molecules. In short, it became apparent that the height of the HATCN (carbon backbone and nitrogen atoms) increased slightly compared to the homomolecular HATCN layer (see Tables S2 and S4, Supporting Information). A detailed inspection of the nitrogen atoms of the cyano groups which are close to the HAT molecules showed that these exhibit a larger distance to the surface than those facing away from the HAT molecule. Furthermore, the average height of the carbon atoms of the HAT molecule decreased upon adsorption close to a HATCN molecule. These structural changes already give a first indication that the HATCN/substrate interaction is decreased when intermixing with the HAT while the HAT/substrate and the intermolecular interaction seem to be increased.

2.3. X-Ray Photoelectron Spectroscopy

Figure 3 shows XPS data for the N 1s and O 1s core levels taken on the homomolecular as well as the intermixed layers. The C 1s spectra are shown in Figure S6 in the Supporting Information. The N 1s spectrum of HATCN shows two components, which were fitted with a 1:1 area ratio. The peak at lower binding energy stems from the cyano component of HATCN while the peak at higher binding energy corresponds to the N-atoms within the backbone of the molecule.[36] The O 1s spectra consist of only one component, which is in line with the chemical structure of the HAT molecule. For the intermixed

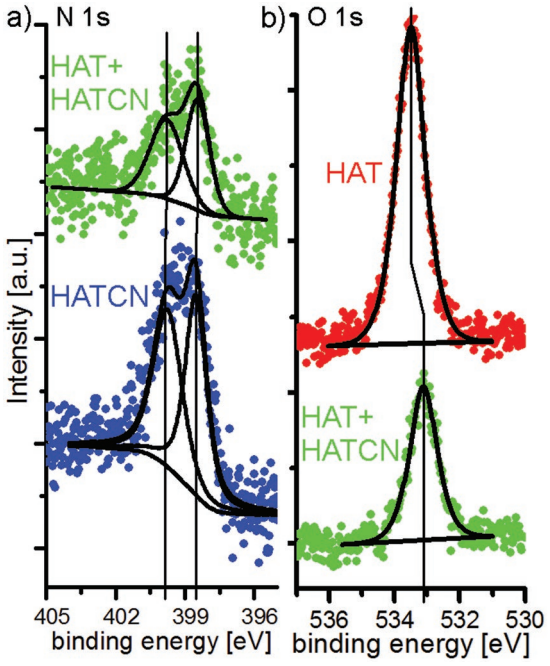

Figure 3. XPS spectra for monolayers of HATCN (blue), HAT+HATCN (green) and HAT (red). a) N 1s spectra, b) O 1s spectra.

© 2019 The Authors. Published by WILEY-VCH Verlag GmbH & Co. KGaA, Weinheim

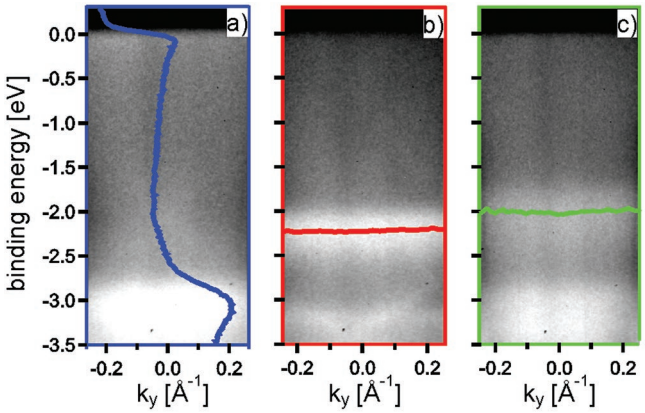

Figure 4. ARPES data taken 5° off-normal emission (k_x = 0.18 Å^{-1}) for a) HATCN, b) HAT and c) HAT+HATCN. The blue line in a) represents the momentum-integrated intensity as a function of the energy. The red and green line in b) and c) indicate the position of the HOMO from the fits (see Supporting Information) in the pure and in the intermixed layer, respectively. The high intensity around −3 eV arises from the Ag 4d bands.

molecular layer, the binding energies of the N 1s peaks of HATCN exhibited almost no shifts. In contrast, the O 1s peak of HAT shifted by 0.4 eV toward lower binding energies when mixing with the acceptor molecule HATCN (see Table S5, Supporting Information). Earlier reports demonstrated a similar shift of donor core levels to lower binding energy when mixing a donor with an acceptor molecule.[9,14,19,27]

When comparing the full-width at half maximum (FWHM) of the peaks it is clearly visible that it is decreased for the N 1s peaks when going from the pure HATCN layer to the intermixed layer (see Table S5, Supporting Information). In contrast, the O 1s peaks of the HAT molecule do not show any significant changes in the FWHM. The implications of the changes of the FWHM will be discussed later.

2.4. Electronic Properties

In a next step, we investigated the electronic properties of the homomolecular as well as the intermixed layers by means of angle-resolved photoelectron spectroscopy (ARPES), UPS, and STS. The ARPES results for monolayer coverage of HATCN are shown in **Figure 4**a. The blue line represents the momentum-integrated intensity as function of the binding energy. A slight increase of the intensity close to the Fermi level was observed. This was also seen by angle-integrated UPS (Figure S7b,d, Supporting Information). We associate the increased intensity around the Fermi level with a partial filling of the LUMO of HATCN, which was also reported in an earlier publication.[34] This partial filling is in line with the Bader charge analysis of our DFT calculations, which showed a charge transfer of 2.3 electrons per molecule from the substrate into the molecule. Our calculation of HATCN's density of states (DOS) also illustrates a shifting of the LUMO toward the Fermi level (see Figure S8a, Supporting Information). The HOMO of the pure HATCN could not be observed in the ARPES/UPS data. The HOMO–LUMO gap of HATCN in the gas phase is 3.3 eV (Figure 1).[31] We, therefore, suspect an overlapping of the HATCN HOMO with the silver 4d bands, which gave rise to a high intensity below −2.8 eV. DFT calculations locate the HOMO of HATCN on the substrate at −2.5 eV (Figure S8a, Supporting Information) providing good qualitative support for this idea considering the well-known fact that DFT underestimates the bandgap, which leads to discrepancies in the calculated and measured DOS.[37]

For approximately one monolayer of HAT, a clear band was found at −2.2 eV (see red line in Figure 4b), which can be associated with the HOMO of the HAT molecule. The HOMO calculated by DFT lies significantly higher in energy at −1.1 eV (Figure S8b, Supporting Information).

In the case of the intermixed molecular layer, a HOMO was observed at −2.0 eV (Figure 4c). We propose that this is the HOMO of HAT shifted by ≈0.2 eV toward the Fermi level when compared to the homomolecular layer. Earlier studies also reported a shift of the donor HOMO level toward the Fermi level for the mixing of a donor with an acceptor molecule.[14,21] Additionally, the HOMO of the intermixed layer was significantly broadened compared to the one of the pure HAT layer (see Figure S10, Supporting Information). Our DFT calculations also indicate a significant broadening in the DOS of the HAT molecule, specifically in the deeper levels, when going from a homomolecular layer to an intermixed molecular layer (peak around −3 eV in Figure S8b, Supporting Information). This clearly reinforces the notion that the HAT molecule interacts more strongly with the surface or its neighboring molecules when it is in the vicinity of HATCN. El-Sayed et al. reported a broader HOMO of the acceptor (fluorinated copperphthalocyanines) molecule in the homomolecular layer while its width decreased by mixing with pentacene as a donor.[22] Furthermore, the increased intensity around the Fermi level observed for HATCN alone was significantly reduced in the intermixed molecular layer (Figure S7b,d, Supporting Information). This demonstrates that the charge transfer between the substrate and HATCN was reduced upon deposition of the electron donating molecule (HAT) indicating a reduced HATCN–substrate interaction. This is in line with our Bader charge analysis, which shows a charge transfer of only 1.4 electrons from the Ag(111) into one HATCN when HATCN is adsorbed close to HAT on the Ag surface.

However, DFT calculations illustrate no changes in the position of the occupied states of both HAT and HATCN when going from the homomolecular layers to the intermixed molecular layer. This is probably due to the simplification of the superstructure used for the calculations, which contains only one HAT and one HATCN molecule while in our unit cell each HAT is surrounded by four HATCN molecules. Therefore, we performed another set of calculations for the intermixed unit cell but without the Ag(111) substrate. Here we observe a significant broadening of all electronic states (Figure S9, Supporting Information) due to the strong interaction between HAT and HATCN, which fits well with the observed broadening of the HOMO shown in Figure S10 in the Supporting Information.

In addition to the ARPES results, we measured work function changes of the homomolecular and intermixed layers, which are summarized in **Table 1** and in Figure S7c in the Supporting Information. UPS measurements and DFT calculations demonstrate that the work function of the HATCN

© 2019 The Authors. Published by WILEY-VCH Verlag GmbH & Co. KGaA, Weinheim

Table 1. Work function changes relative to the clean Ag(111) substrate derived from UPS and from DFT.

	HATCN	HAT	HAT+HATCN
Work function changes [eV] from UPS	0.0	−0.9	−0.4
Work function changes [eV] from DFT	+0.1	−0.9	−0.3

monolayer on Ag(111) is similar to the one of the clean substrate, which is in line with earlier reports.[38] Our DFT calculations even showed a slight increase of the work function by 0.1 eV compared to the one of clean Ag(111). In contrast, the work function strongly decreased by 0.9 eV upon adsorption of a HAT monolayer on Ag(111). The work function of the intermixed layer resides between those of the homomolecular layers. Generally, the work function of a substrate decreases upon the adsorption of organic molecules due to Pauli repulsion between the electron cloud of the metal and the electrons from the adsorbates. This effect can explain the reduction of the work function observed for monolayer coverage of HAT. For the monolayer of HATCN, the Pauli repulsion is counteracted by the charge transfer from the substrate to the HATCN molecules, as observed by ARPES/UPS measurements and DFT calculations, leading to a surface dipole.

Our observations of the work function changes can be well described by a method used by Goiri et al.[9] and El-Sayed et al.[14] For weakly interacting, bi-component systems the work function change of an intermixed molecular layer can be determined by the work function changes of the pure components as long as the surface areas occupied by the adsorbates are known. By deriving the surface area values from the unit cell parameters, we calculated a theoretical work function change of 0.43 eV (see Table S6 in the Supporting Information for details). This value is very close to the measured value of −0.4 eV showing that according to this method our system behaves similarly to the previously reported donor/acceptor systems.[9,15]

In order to investigate the electronic properties on a local scale, STS was performed for the homomolecular and the intermixed phases. The results are summarized in **Figure 5**. We focused on the unoccupied electronic states since the HOMO positions could be derived from the ARPES and UPS data. STS for the homomolecular HATCN layer shows that the surface state of Ag(111) is shifted into the unoccupied states by around 80 mV with respect to the clean Ag(111) surface state (dark blue line, Figure 5 and Figure S11b, Supporting Information). Additionally, a small feature 70 mV below the Fermi level is visible in the spectrum. We ascribe this to partial charge transfer from the Ag surface into the molecule, in line with our ARPES and work function measurements.[39] No further features were found in the STS spectra for the HATCN molecules within the investigated energy range.

For the homomolecular layer of HAT, an even stronger shift of the surface state of ≈150 mV into the unoccupied states was observed (red line, Figure 5 and Figure S11b, Supporting Information). Besides the shift of the surface state, a dip around 0.75 V in the density of states was found. We assume that the LUMO resides just below this dip around 0.65 V where a small increase in the DOS is visible. The intense background above 0.2 eV can be assigned to the remaining Shockley surface state of Ag(111), whose intensity only decreases slightly with increasing voltage.[40]

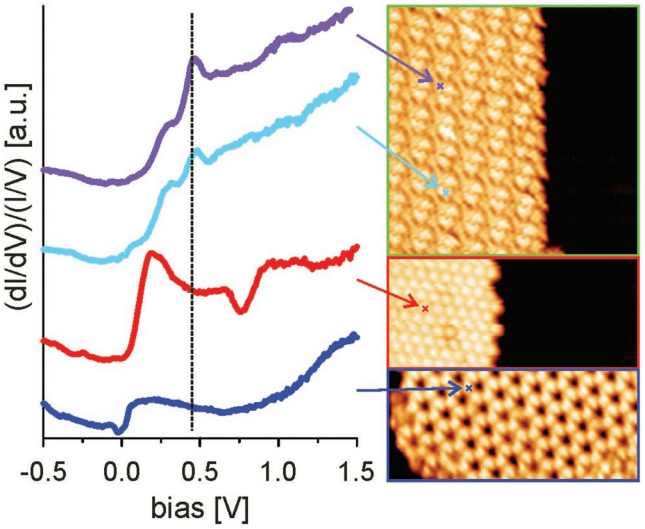

Figure 5. STS data for the homomolecular HATCN and HAT islands (dark blue and red curve, respectively) and for the HATCN (light blue) as well as HAT (purple) molecule in the intermixed layer acquired at 5 K. The dotted black line at 0.45 V indicates the position at which the d*I*/d*V* map in Figure 6 was taken. The panel on the right shows the corresponding STM images. The colored crosses indicate at which positions the d*I*/d*V* spectra were taken. (Bottom right: HATCN 22 × 10 nm^2; center right: HAT 15.6 × 6.7 nm^2; top right: intermixed island 20 × 20 nm^2; set-points: $U = -0.5$ V, $I = 200$ pA for pure HAT and pure HATCN, $U = +0.5$ V, $I = 200$ pA for the intermixed island).

When probing the electronic properties of the molecules in the intermixed layer, clear differences were observed compared to the homomolecular layers. First of all, the Ag(111) surface state seems to be quenched in the intermixed layer (Figure S11b, Supporting Information). Second, there is qualitatively no difference between the STS spectra acquired either on top of HAT molecules or on top of HATCN molecules (Figure 5, two top most spectra). Both exhibited an increase in the density of states around 0.2 V. The clear peak at around 0.45 V can be assigned to an unoccupied molecular orbital (dotted black line). Note that neither HAT nor HATCN in the homomolecular layers showed a similar feature.

Noteworthy, our DFT calculations of the intermixed layer without the Ag(111) substrate also show significant changes in the molecular orbitals compared to the calculations of the single molecules (Figure S9, Supporting Information). In detail, a broadening of most of the states is visible. Furthermore, some states of the HAT and HATCN overlap, which might be an indication for the hybridization between the molecules. Last but not least, the calculations of the CT complex show a charge transfer of 0.4 electrons from the HAT into the HATCN.

In order to determine the local distribution of this unoccupied molecular orbital, d*I*/d*V* maps were taken at 0.45 V for the intermixed phase. It is clearly visible that the cross-like HAT molecules in the intermixed layer appear brighter in the d*I*/d*V* map, i.e., they exhibit a higher conductivity than the triangular HATCN molecules (**Figure 6**). This was also visible in the d*I*/d*V* spectra where the peak at 0.45 eV showed more intensity

© 2019 The Authors. Published by WILEY-VCH Verlag GmbH & Co. KGaA, Weinheim

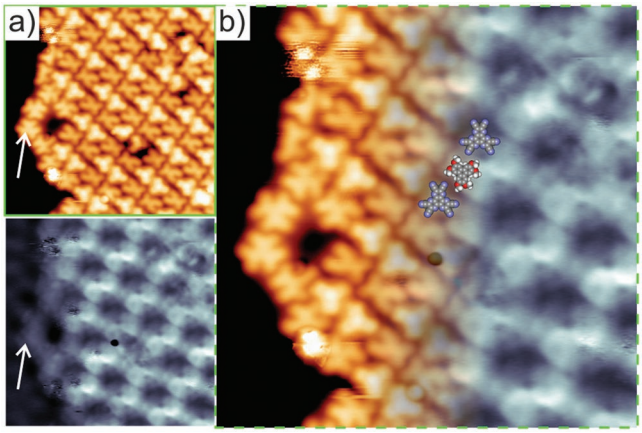

Figure 6. STM image and simultaneously acquired d*I*/d*V* map of the intermixed layer taken at a bias of 0.45 V as indicated by the vertical line in Figure 5, acquired at 5 K. a) Top: topography, bottom: d*I*/d*V* map. The white arrows point to a row of HAT molecules at the border of the island, which exhibit lower conductivity. b) Superposition of the topography and the d*I*/d*V* map (12×12 nm^2, $I = 200$ pA). The positions of a few molecules are sketched.

on top of the HAT molecule than on top of the HATCN molecule (Figure 5 and Figure S11a, Supporting Information). Interestingly, HAT molecules at the boarder of the intermixed island, which are not in contact with HATCN molecules (white arrows in Figure 6a) displaying the six-leg structure, exhibited a reduced conductivity compared to the molecules within the intermixed structure. This further indicates that the electronic structure of HAT changed upon mixing of the two molecules. Note that at the homogeneously mixed borders of the islands the conductivity is the same as in the center of the island (see Figure S12, Supporting Information). Thus, we exclude a spill-out effect, which might have induced this weaker contrast for the HAT molecules at the island borders. From the STS data, we conclude that the two molecules hybridize in the intermixed layer leading to an alignment of the unoccupied molecular orbitals. This is in contrast to weakly interacting organic donor/acceptor systems like the combination of CuPc and F_{16}CuPc on graphite where shifts of the HOMO and LUMO positions have been observed but no common molecular orbitals for both donor and acceptor molecules were reported.[21]

3. Discussion

Figure 7 depicts the energy levels of the homomolecular layers of the acceptor HATCN and the donor HAT and compares them to the energy levels of the intermixed molecular layer. The energy values were derived from the above reported ARPES/UPS, STS, and XPS measurements and are displayed with respect to the Fermi level. For weak interacting organic donor/acceptor systems, a rigid shift away from the vacuum level was usually reported when increasing the donor/acceptor ratio.[9,14,18] This was described by the so-called vacuum level pinning (VLP) model where all energies (conduction band, valence band, and core levels) are pinned to the vacuum level.[9,14] In other words, if the work function is reduced, all energy levels will be shifted to lower values by a similar amount. This seems to be the case for the HAT molecule. The work function compared to the intermixed layer is reduced by 0.5 eV and the HOMO as well as the O 1s core level were shifted away from the Fermi level, although the shift of the HOMO only amounted to approximately half of the shift of the vacuum level and the O 1s binding energy.

In the case of HATCN one might expect a Fermi level pinning (FLP) instead of a VLP.[14] This means that the work function decrease caused by the mixing of the two molecules is counteracted by a small charge redistribution of the partially filled LUMO at the Fermi level leaving the energetic positions of the HATCN states unaffected. Indeed, we observed a decreased intensity close to the Fermi level in the mixed layer compared to the pure HATCN indicating a charge redistribution (Figure S7d, Supporting Information). Additionally, the N 1s core levels did not show any significant changes in binding energy for the homomolecular and mixed layer, which is an indication for FLP.

However, the simple picture of the VLP or the FLP model fails to explain the hybridization of the donor and acceptor molecules leading to the alignment of the unoccupied molecular orbitals as observed in the STS measurements (Figure 5). Our STS data showed that the electronic structure of the unoccupied states of both HAT and HATCN in the intermixed layer were similar. For both molecules a LUMO peak at 0.45 V was detected, which was observed neither for the homomolecular HAT nor for the homomolecular HATCN layer. Furthermore, the LUMO of HAT compared to the intermixed layer shifted toward E_{vac} by 0.2 eV while all other states showed a shift in the opposite direction.

Our combined ARPES and DFT data show that HATCN exhibited a significant interaction with the Ag(111) surface in the homomolecular layer leading to a substantial charge transfer. In contrast, as indicated by our DFT calculations for gas phase and adsorbed HAT molecules in the homomolecular layer, the structural and electronic properties of HAT were essentially unaffected upon adsorption on the Ag(111) (see Supporting Information). Intermixing HATCN and HAT

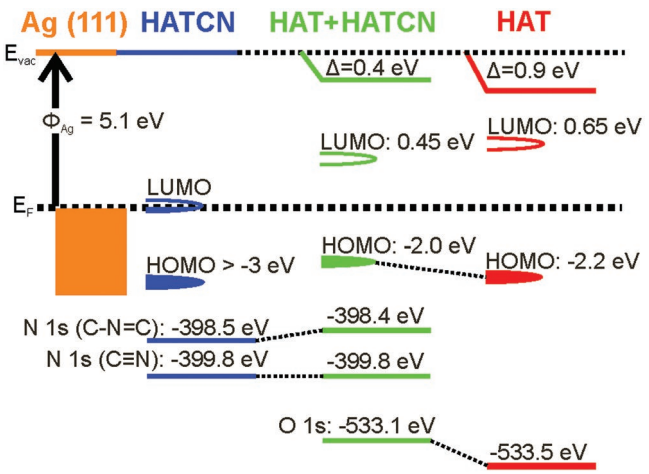

Figure 7. Energy levels (not drawn to scale) for HATCN and HAT and the intermixed phase on Ag(111), as derived from XPS, ARPES/UPS, and STS measurements.

© 2019 The Authors. Published by WILEY-VCH Verlag GmbH & Co. KGaA, Weinheim

led to hybridization between the two molecules evidenced in the emergence of the new common LUMO, which shows a spatially homogeneous distribution across both molecules and a broadening of the molecular electronic states and a charge transfer from the HAT to the HATCN as observed by our DFT calculations. Finally, the hybridization was accompanied by a conformational change of HAT as can be seen from the STM data. We assume that in the intermixed layer the intermolecular interactions are considerably stronger than the molecule/substrate interactions, also because the assemblies changed from commensurate in the homomolecular layers to incommensurate in the intermixed layer. The increased intermolecular interactions were also manifested in a broadening of HAT's occupied states visible in the ARPES and DFT data (Figures S8–S10, Supporting Information). Furthermore, we observed a reduced HATCN–substrate interaction in the intermixed layer which resulted in a decreased FWHM of the N 1s and C 1s core levels in the intermixed layer, in a reduced charge transfer from the substrate into the HATCN and an increased adsorption height of the HATCN molecule (see Figure S7d and Tables S2, S4 and S5, Supporting Information).

4. Conclusion

In conclusion, we studied two structurally and electronically complementary organic molecules on Ag(111). Both molecules assembled into well-ordered, commensurate structures for monolayer deposition. The electron donor HAT showed weak interaction with the Ag(111) surface, while for the electron acceptor HATCN buckling and charge transfer into the LUMO were observed upon adsorption. By intermixing the two molecules, we found a strong hybridization leading to the emergence of a common unoccupied state, which was not present for the homomolecular layers. Additionally, we gained strong evidence that the intermolecular interactions strongly increased in the intermixed layer while the HATCN-substrate interaction decreased significantly. This is corroborated by our DFT calculations, which show a charge transfer from the HAT into the HATCN for the intermixed superstructure and by our UV–vis data of the solid CT complex which exhibits hybrid states. Our surface supported HATCN/HAT system, therefore, represents a CT complex suitable for possible usage in organic (opto)electronics.

5. Experimental Section

Synthesis and Electrochemical Measurements: HATCN and HAT were synthesized according to literature procedures.[41] Cyclic voltammetry measurements were performed on a computer-controlled BAS CV-50W instrument at ambient probe temperature in CH_2Cl_2 solutions containing 0.1 M *n*-Bu_4NPF_6 as supporting electrolyte at a scan rate of 100 mV s^{-1}. A Pt wire was used as a counter electrode, $Ag/AgNO_3$ as a reference electrode, and Pt as a working electrode. UV–vis was performed on the pure HAT and HATCN dissolved in MeCN solution with a concentration of $\approx 4 \times 10^{-6}$ M with an Agilent Technologies, Cary 60 spectrophotometer. The sample containing HAT+HATCN (3 mg mL^{-1}) was deposited on 2 cm × 2 cm glass wafer in commercially available PMMA as matrix (Sigma) dissolved in MeCN. A table top spin coater from S.P.S (Spin 150) was used and 11 mg of PMMA were dissolved in 1 mL of warm MeCN prior to the sample preparation. UV–vis absorption spectra were recorded on a JASCO V-670 spectrophotometer by fixating the coated glass wafer in the beam path. An uncoated wafer was used as reference.

Sample Preparation: All experiments were carried out under ultra-high vacuum (UHV) conditions. Ag(111) single crystals were cleaned by repeated cycles of Argon ion sputtering and subsequent annealing at 400 °C. The sample quality was checked by STM, XPS, or LEED prior to molecule deposition. Molecules were deposited with a Knudsen cell evaporator while the substrate was kept at room temperature and the evaporation rate was monitored by means of a quartz crystal microbalance. Typical evaporation rates were in the range of 0.2–0.5 ML min^{-1}, where one monolayer corresponds to full coverage of the surface with the (7 × 7) and $\left(\sqrt{21}\times\sqrt{21}\right)R10.9°$ overlayer for HATCN and HAT, respectively. For the preparation of the intermixed structure, HAT molecules were deposited first followed by HATCN molecules. In order to improve the quality of the mixed layers for surface averaging measurements like XPS, ARPES, and UPS, the samples were annealed at 150 °C after deposition of both molecules. The samples did not undergo any annealing for STM and STS measurements.

STM and STS Measurements: STM and STS measurements were performed in a two chamber UHV system equipped with a commercial low-temperature STM/AFM and a MCP LEED optics (Scienta Omicron GmbH). STM images were either acquired at 77 K or at 5 K using a mechanically cut Pt/Ir tip. The bias voltages in the text are given with respect to a grounded tip. STS measurements were performed with an external lock-in amplifier using a lock-in frequency of 678 Hz and a modulation voltage of 12 mV (rms-value) at liquid helium temperatures (5 K). WSxM was used to analyze the STM images.[42]

UPS and Work Function Measurements: UPS and work function measurements were carried out in a separate UHV system equipped with a variable temperature STM (Scienta Omicron GmbH), a hemispherical energy analyzer (Thermo Fisher), a twin anode X-ray source, a He discharge lamp, and LEED optics (SPECS). The STM was used to confirm that at least 90% of the surface was covered with molecules to ensure a reasonable intensity for spectroscopy measurements. For the measurements of the intermixed samples, at least 90% of the molecules were arranged in the above described mixed structure. The overall quality of the samples was determined with LEED. UPS was performed by using a nonmonochromatized HeI lab source (21.2 eV) under an angle of ≈30° with respect to the surface normal and with an acceptance angle of ≈12°. Work function measurements were performed by applying a bias of −5 V to the sample and measuring the secondary electron cut-off and the Fermi level.

XPS and ARPES Measurements: XPS and ARPES measurements were performed in a multichamber UHV system equipped with an analyzer chamber containing a SPECS 150 hemispherical analyzer. ARPES measurements were performed with monochromatized HeI radiation (21.2 eV) under an angle of 5° with respect to the surface normal in order to remove the intensity coming from the surface state of the Ag(111). In a connected chamber, a Kratos Axis Ultra XPS system containing a monochromatized Al K_α X-ray source was used to acquire high-resolution XPS data. The preparation chamber contained LEED optics (SPECS). However, the system did not contain a STM to monitor the structural quality of the samples. Hence, coverage and quality of the molecular films were investigated in different ways. First, the amount of molecules necessary for 1 ML of HAT could be estimated by LEED as the molecules were mobile at room temperature for coverages below 1 ML and only for coverages close to 1 ML a sharp LEED pattern could be observed. Second, the molecular coverage was determined by monitoring the silver surface state with ARPES, which was shifted into the unoccupied states for samples covered with a full monolayer of molecules. A weak remainder of the original silver surface state indicated that the surface was almost completely covered with molecules, without having a second molecular layer. Finally, the quality of the LEED pattern for the intermixed structure and absence of LEED spots related to pure HAT or HATCN domains was used to confirm that the majority of the sample was covered by the above-described intermixed phase.

The binding energy of the XPS data was referenced to the Ag $3d_{5/2}$ peak at 368.3 eV.[43] Subtraction of the silver plasmon peaks,

© 2019 The Authors. Published by WILEY-VCH Verlag GmbH & Co. KGaA, Weinheim

which overlap with the N 1s region, was carried out in the following way. The N 1s background region was measured for one monolayer of HAT molecules, which do not contain any nitrogen.[44] This spectrum was smoothed, the intensities of all spectra were aligned at the low binding energy site of the region, and then the background spectrum was subtracted from the data measured for HATCN and for the intermixed layer. For all spectra a Shirley-type background was subtracted except for the O 1s region where a linear background was employed. The peaks were fitted by a combination of Lorentzian and Gaussian functions. The area ratios for the N 1s spectra and the C 1s spectra were constrained according to the structural formulas of the molecules. The ARPES data were fitted by a simple Lorentzian function after subtraction of a linear background (see Supporting Information for more details).

Computational Methods: Density functional theory calculations were performed using the VASP code (version 5.4.4),[45] which used the projector augmented wave (PAW) method.[46] For the bulk lattice constant of Ag the calculated value of 4.147 Å was used.[47] For structural relaxation, the optB88-vdW functional was opted,[48] which includes the van der Waals (vdW) interaction through a nonlocal contribution to the correlation energy. Several investigations revealed that the optB88 functional provided an overall good agreement with experimental results.[47,49] For calculating the work function, the PBE functional was used.[50] The plane wave energy cut-off was set at 400 eV, and structural relaxation was achieved using a force criterion of 0.01 eV $Å^{-1}$. For all calculations, Monkhorst–Pack sampling was used. For the calculations of the adsorbed molecules, a $14 \times 14 \times 14$ grid was used while for bulk calculations a $3 \times 3 \times 1$ and a $2 \times 2 \times 1$ grid were used for HAT and HATCN, respectively. In agreement with the experimental observations, a 7×7 overlayer was constructed for HATCN and a $\left(\sqrt{21} \times \sqrt{21}\right) R10.9°$ one for HAT. For the HATCN and HAT calculations, four layers were used with 49 atoms/layer for HATCN and 21 atoms/layer for HAT, where the HATCN unit cell contained two molecules and the HAT unit cell one molecule. For the intermixed phase, a substrate was created containing three layers and 60 atoms per layer. On that specific substrate, one HAT and one HATCN molecule were positioned. The supercell used in all the calculations contained at least 20 Å of vacuum separation. For the calculations of the intermixed phase without the Ag substrate, a unit cell of 2.4 nm × 2.7 nm with an angle of 77° similar to the one found in STM for the intermixed structure was used.

Supporting Information

Supporting Information is available from the Wiley Online Library or from the author.

Acknowledgements

J.C. Moreno-Lopez, M. Enache, and S. Gottardi are acknowledged for their help during the experiments. M. Grunst is acknowledged for his support during the synthesis and characterization of HATCN. R. Gutzler is acknowledged for discussions and proofreading of the manuscript. This work was supported by the Netherlands Organisation for Scientific Research (NWO) (Chemical Sciences, VIDI-grant No. 700.10.424 and VENI-grant No. 722.012.010), by the European Research Council (ERC-2012-StG307760-SURFPRO), and by the Zernike Institute for Advanced Materials of the University of Groningen. M.K. gratefully acknowledges funding by the Deutsche Forschungsgemeinschaft (DFG)–Projektnummer 182849149–SFB 953 and Projektnummer 401247651–KI1662/3-1. W.M., A.K., and K.L. acknowledge support from the U.S. Department of Energy Basic Energy Science under Contract No DE-FG02-11ER16243. This research used resources of the National Energy Research Scientific Computing Center, which is supported by the Office of Science of the U.S. Department of Energy.

Conflict of Interest

The authors declare no conflict of interest.

Keywords

acceptor molecules, charge-transfer complex, donor molecules, photoelectron spectroscopy, scanning tunneling microscopy and spectroscopy, self-assembly

Received: April 5, 2019
Revised: June 14, 2019
Published online: July 2, 2019

[1] a) F. Reineke, F. Lindner, G. Schwartz, N. Seidler, K. Walzer, B. Lüssem, K. Lei, *Nature* **2009**, *459*, 234; b) J.-H. Jou, S. Sahoo, K. K. Dubey, R. A. K. Yadav, S. S. Swayamprabha, S. D. Chavhan, *J. Mater. Chem. C* **2018**, *6*, 11492.
[2] a) S. Fukuzumi, T. Kojima, *J. Mater. Chem.* **2008**, *18*, 1427; b) L. Xu, C.-L. Ho, L. Liu, W.-Y. Wong, *Coord. Chem. Rev.* **2018**, *373*, 233.
[3] a) G. Horowitz, *Adv. Mater.* **1998**, *10*, 365; b) J. Zhang, W. Xu, P. Sheng, G. Zhao, D. Zhu, *Acc. Chem. Res.* **2017**, *50*, 1654.
[4] a) P. Lin, F. Yan, *Adv. Mater.* **2012**, *24*, 34; b) R. Paolesse, S. Nardis, D. Monti, M. Stefanelli, C. Di Natale, *Chem. Rev.* **2017**, *117*, 2517.
[5] C. R. Kagan, D. B. Mitzi, C. D. Dimitrakopoulos, *Science* **1999**, *286*, 945.
[6] a) R. Otero, A. L. Vázquez de Parga, J. M. Gallego, *Surf. Sci. Rep.* **2017**, *72*, 105; b) H. Liang, Y. He, Y. Ye, X. Xu, F. Cheng, W. Sun, X. Shao, Y. Wang, J. Li, K. Wu, *Coord. Chem. Rev.* **2009**, *253*, 2959; c) M. Koepf, F. Chérioux, J. Wytko, J. Weiss, *Coord. Chem. Rev.* **2012**, *256*, 2872.
[7] H. Ishii, K. Sugiyama, E. Ito, K. Seki, *Adv. Mater.* **1999**, *11*, 605.
[8] a) J. L. Zhang, S. Zhong, J. Q. Zhong, T. C. Niu, W. P. Hu, A. T. S. Wee, W. Chen, *Nanoscale* **2015**, *7*, 4306; b) C. Steiner, Z. Yang, B. D. Gliemann, U. Meinhardt, M. Gurrath, M. Ammon, B. Mayer, M. Kivala, S. Maier, *Chem. Commun.* **2018**, *54*, 11554.
[9] E. Goiri, P. Borghetti, A. El-Sayed, E. Ortega, D. G. de Oteyza, *Adv. Mater.* **2016**, *28*, 1340.
[10] X. Bouju, C. Mattioli, G. Franc, A. Pujol, A. Gourdon, *Chem. Rev.* **2017**, *117*, 1407.
[11] a) P. Marmot, N. Battaglini, P. Lang, G. Horowitz, J. Hwang, A. Kahn, C. Amato, P. Calas, *Org. Electron.* **2008**, *9*, 419; b) S. Braun, W. R. Salaneck, M. Fahlman, *Adv. Mater.* **2009**, *21*, 1450.
[12] a) J. A. Theobald, N. Oxtoby, M. A. Phillips, N. R. Champness, P. H. Beton, *Nature* **2003**, *424*, 1029; b) G. M. Whitesides, E. E. Simanek, J. P. Mathias, C. T. Seto, D. N. Chin, M. Mammen, D. M. Gordon, *Acc. Chem. Res.* **1995**, *28*, 37; c) A. Llanes-Pallas, M. Matena, T. Jung, M. Prato, M. Stöhr, A. Bonifazi, *Angew. Chem.* **2008**, *120*, 7840; *Angew. Chem., Int. Ed.* **2008**, *47*, 7726; d) N. Gonzalez-Lakunza, M. E. Cañas-Ventura, P. Ruffieux, R. Rieger, K. Müllen, R. Fasel, A. Arnau, *ChemPhysChem* **2009**, *10*, 2943.
[13] a) D. G. de Oteyza, J. M. Garcia-Lastra, E. Goiri, A. El-Sayed, J. E. Ortega, *J. Phys. Chem. C* **2014**, *118*, 18626; b) E. Barrena, D. G. de Oteyza, H. Dosch, Y. Wakayama, *ChemPhysChem* **2007**, *8*, 1915.
[14] A. El-Sayed, P. Borghetti, E. Goiri, C. Rogero, L. Floreano, G. Lovat, D. J. Mowbray, J. L. Cabellos, Y. Wakayama, A. Rubito, J. E. Ortega, D. G. de Oteyza, *ACS Nano* **2013**, *7*, 6914.
[15] E. Goiri, M. Matena, A. El-Sayed, J. Lobo-Checa, P. Borghetti, C. Rogero, B. Betlefs, J. Duvernay, J. E. Ortega, D. G. de Oteyza, *Phys. Rev. Lett.* **2014**, *112*, 117602.

© 2019 The Authors. Published by WILEY-VCH Verlag GmbH & Co. KGaA, Weinheim

[16] Y. L. Huang, W. Chen, H. Li, J. Ma, J. Pflaum, A. T. S. Wee, *Small* **2010**, *6*, 70.
[17] a) P. Borghetti, A. El-Sayed, E. Goiri, C. Rogero, J. Lobo-Check, L. Floreano, J. E. Ortega, D. M. de Oteyza, *ACS Nano* **2014**, *8*, 12786; b) D. G. de Oteyza, J. M. García-Lastra, M. Corso, B. P. Doyle, L. Floreano, A. Morgante, Y. Wakayama, A. Rubio, J. E. Ortega, *Adv. Funct. Mater.* **2009**, *19*, 3567; c) D. G. de Oteyza, I. Silanes, M. Ruiz-Osés, E. Barrena, B. P. Boyle, A. Arnau, H. Dosch, Y. Wakayama, J. E. Ortega, *Adv. Funct. Mater.* **2009**, *19*, 259.
[18] P. Borghetti, D. G. de Oteyza, C. Rogero, E. Goiri, A. Verdini, A. Cossaro, L. Floreano, J. E. Ortega, *J. Phys. Chem. C* **2016**, *120*, 5997.
[19] Y. Wakayama, D. G. de Oteyza, J. M. Garcia-Lastra, K. J. Mowbray, *ACS Nano* **2011**, *5*, 581.
[20] J. L. Cabellos, D. Mowbray, E. Goiri, A. El-Sayed, L. Floreano, D. G. de Oteyza, C. Rogero, J. E. Ortega, A. Rubio, *J. Phys. Chem. C* **2012**, *116*, 17991.
[21] J.-Q. Zhong, X. Qin, J.-L. Zhang, S. Kera, N. Ueno, A. T. S. Wee, J. Yang, W. Chen*ACS Nano* **2014**, *8*, 1699.
[22] A. El-Sayed, D. J. Mowbray, J. M. Gardcía-Lastra, C. Rogero, E. Goiri, P. Borghetti, A. Turak, B. P. Doyle, M. Dell'Angela, L. Floreano, Y. Wakayama, A. Rubio, J. E. Ortega, D. G. de Oteyza, *J. Phys. Chem. C* **2012**, *116*, 4780.
[23] N. Gonzalez-Lakunza, I. Fernández-Torrente, K. J. Franke, N. Lorente, A. Arnau, J. I. Pascual, *Phys. Rev. Lett.* **2008**, *100*, 156805.
[24] J. Ferraris, D. O. Cowan, V. Walatka, J. H. Perlstein, *J. Am. Chem. Soc.* **1973**, *95*, 948.
[25] a) K. Medjanik, D. Chercka, P. Nagel, M. Merz, S. Schuppler, M. Baumgarten, K. Müllen, S. A. Nepijko, H.-J. Elmers, G. Schönhense, H. O. Jeschke, R. Valenti, *J. Am. Chem. Soc.* **2012**, *134*, 4694; b) K. Medjanik, A. Gloskovskii, D. Kutnayakhov, C. Felser, D. Chercka, M. Baumgarten, K. Müllen, G. Schönhense, *J. Electron Spectrosc. Relat. Phenom.* **2012**, *185*, 77.
[26] K. Medjanik, S. Perker, S. Naghavi, M. Rudloff, V. S. D. Chercka, M. Huth, S. A. Nepijko, R. Methfessel, C. Felser, M. B. K. Müllen, H. J. Elmers, G. Schönhense, *Phys. Rev. B* **2010**, *82*, 245419.
[27] K. Medjanik, D. Kutnyakhov, S. A. Nepijko, G. Schönhense, S. Naghavi, V. Alijani, C. Felser, N. Koch, R. Rieger, M. Baumgarten, K. Müllen, *Phys. Chem. Chem. Phys.* **2010**, *12*, 7184.
[28] a) B. Kurpil, A. Savateev, V. Papaefthimiou, S. Zafeiratos, T. Heil, X. Özenler, D. Dontsova, M. Antonietti, *Appl. Catal., B* **2017**, *217*, 622; b) V. Lemaur, D. A. da Silva Filho, V. Coropceanu, M. Lehmann, Y. Geerts, J. Priris, M. G. Debije, A. M. van de Craats, K. Senthilkumar, A. K. Siebbeles, J. M. Warman, J.-L. Brédas, J. Cornil, *J. Am. Chem. Soc.* **2004**, *126*, 3271.
[29] L. Y. Park, D. G. Hamilton, E. A. McGehee, K. A. McMenimen, *J. Am. Chem. Soc.* **2003**, *125*, 10586.
[30] M. Schubert, P. Franzmann, A. Wünsche von Leupoldt, K. Koszinowski, K. Heinze, S. R. Waldvogel, *Angew. Chem.* **2016**, *128*, 1168; *Angew. Chem., Int. Ed.* **2016**, *55*, 1156.
[31] C. Falkenberg, S. Olthof, R. Rieger, M. Baumgarten, K. Muellen, K. Leo, M. Riede, *Sol. Energy Mater. Sol. Cells* **2011**, *95*, 927.
[32] a) S. Gottardi, K. Müller, J. C. Moreno-López, H. Yildirim, U. Meinhardt, M. Kivala, A. Kara, M. Stöhr, *Adv. Mater. Interfaces* **2014**, *1*, 1300025; b) K. Müller, J. C. Moreno-López, S. Gottardi, U. Meinhardt, H. Yildirim, A. Kara, M. Kivala, M. Stöhr, *Chem. - Eur. J.* **2016**, *22*, 581.
[33] P. A. Wood, S. J. Vorwick, D. J. Watkin, W. D. S. Motherwell, F. H. Allen, *Acta Crystallogr., Sect. B: Struct. Sci.* **2008**, *64*, 393.
[34] H. Glowatzki, B. Bröker, R.-P. Blum, O. T. Hofmann, A. Vollmer, R. Rieger, K. Müllen, E. Zojer, J. P. Rabe, N. Koch, *Nano Lett.* **2008**, *8*, 3825.
[35] While the unit cell parameters of the pure HATCN and HAT phases where determined from the commensurate superstructures found in LEED by using the lattice constant of Ag of 4.09 Å, the unit cell for the intermixed molecular layer was derived from the STM images. Consequently, the latter one exhibits some errors.
[36] C. Christodoulou, A. Giannakopoulos, M. V. Nardi, G. Ligorio, M. Oehzelt, L. Chen, L. Pasquali, M. Timpel, A. Giglia, S. Nannarone, P. Norman, M. Linares, K. Parvez, K. Müllen, D. Beljonne, N. Koch, *J. Phys. Chem. C* **2014**, *118*, 4784.
[37] a) H. Xiao, J. Tahir-Kheli, W. A. Goddard, *J. Phys. Chem. Lett.* **2011**, *2*, 212; b) J. P. Perdew, W. Yang, K. Burke, Z. Yang, E. K. U. Gross, M. Scheffler, G. E. Scuseria, T M. Henderson, I. Y. Zhang, A. Ruzsinszky, H. Peng, J. Xun, E. Trushin, A. Görling, *Proc. Natl. Acad. Sci. USA* **2017**, *114*, 2801; c) J. M. Crowley, J. Tahir-Kheli, W. A. Goddard III, *J. Phys. Chem. Lett.* **2016**, *7*, 1198.
[38] J. Niederhausen, P. Amsalem, J. Frisch, A. Wilke, A. Vollmer, R. Rieger, K. Müllen, J. P. Rabe, N. Koch, *Phys. Rev. B* **2011**, *84*, 165302.
[39] We can exclude that the dip at the Fermi level is coming from a Kondo effect since the same feature was also observed for STS measurements at liquid nitrogen temperature and it would be expected that the Kondo resonance is strongly reduced at higher temperature.
[40] We exclude a significant charge transfer between Ag(111) and HAT as determined from DFT calculations.
[41] a) J. T. Rademacher, K. Kanakarajan, A. W. Czarnik, *Synthesis* **1994**, *4*, 378; b) S. J. Mahoney, M. M. Ahmida, H. Kayal, N. Fox, Y. Shimizu, S. H. Eichhorn, *J. Mater. Chem.* **2009**, *19*, 9221; c) H. Naarmann, M. Hanack, R. A. Mattmer, *Synthesis* **1994**, *5*, 477.
[42] I. Horcas, R. Fernández, J. M. Gómez-Rodríguez, J. Colchero, J. Gómez-Herrero, A. M. Baro, *Rev. Sci. Instrum.* **2007**, *78*, 013705.
[43] J. F. Moulder, W. F. Stickle, P. E. Sobol, K. D. Bomben, *K. D. Handbook of X-ray Photoelectron Spectroscopy* (Eds.: J. Chastain), Perkin Elmer, Eden Prairie USA, **1992**.
[44] A surface covered with one monolayer of molecules was used as reference instead of the clean silver surface, in order to account for the quenching of the silver Plasmon by the adsorbed molecules.
[45] a) G. Kresse, J. Furthmüller, *Phys. Rev. B* **1996**, *54*, 11169; b) G. Kresse, J. Furthmüller, *Comput. Mater. Sci.* **1996**, *6*, 15; c) G. Kresse, J. Hafner, *Phys. Rev. B* **1993**, *47*, 558.
[46] a) P. E. Blöchl, *Phys. Rev. B* **1994**, *50*, 17953; b) G. Kresse, D. Joubert, *Phys. Rev. B* **1999**, *59*, 1758.
[47] H. Yildirim, T. Greber, A. Kara, *J. Phys. Chem. C* **2013**, *117*, 20572.
[48] J. Klimes, D. R. Bowler, A. Michaelides, *J. Phys.: Condens. Matter* **2010**, *22*, 022201.
[49] a) H. Yildirim, A. Kara, *J. Phys. Chem. C* **2013**, *117*, 2893; b) H. Yildirim, J. Matos, A. Kara, *J. Phys. Chem. C* **2015**, *119*, 25408; c) J. Matos, H. Yildirim, A. Kara, *J. Phys. Chem. C* **2015**, *119*, 1886; d) A. Thomas, W. Malone, T. Leoni, A. Ranguis, Z. Chen, O. Siri, A. Kara, P. Zeppenfeld, C. Becker, *J. Phys. Chem. C* **2018**, *122*, 10828; e) W. Malone, J. Matos, A. Kara, *Surf. Sci.* **2018**, *669*, 121.
[50] J. P. Perdew, K. Burke, M. Ernzerhof, *Phys. Rev. Lett.* **1996**, *77*, 3865.

© 2019 The Authors. Published by WILEY-VCH Verlag GmbH & Co. KGaA, Weinheim